Multiparticle Quantum Walks and Fisher Information in One-Dimensional Lattices

Xiaoming Cai,[1] Hongting Yang,[2] Hai-Long Shi,[1,3] Chaohong Lee,[4,5,*] Natan Andrei,[6] and Xi-Wen Guan[1,7,8,†]
[1]State Key Laboratory of Magnetic Resonance and Atomic and Molecular Physics, Wuhan Institute of Physics and Mathematics, APM, Chinese Academy of Sciences, Wuhan 430071, China
[2]School of Science, Wuhan University of Technology, Wuhan 430071, China
[3]University of Chinese Academy of Sciences, Beijing 100049, China
[4]Guangdong Provincial Key Laboratory of Quantum Metrology and Sensing & School of Physics and Astronomy, Sun Yat-Sen University (Zhuhai Campus), Zhuhai 519082, China
[5]State Key Laboratory of Optoelectronic Materials and Technologies, Sun Yat-Sen University (Guangzhou Campus), Guangzhou 510275, China
[6]Department of Physics, Rutgers University, Piscataway, New Jersey 08854, USA
[7]NSFC-SPTP Peng Huanwu Center for Fundamental Theory, Xi'an 710127, China
[8]Department of Theoretical Physics, Research School of Physics and Engineering, Australian National University, Canberra ACT 0200, Australia

(Received 21 January 2021; revised 19 February 2021; accepted 4 August 2021; published 3 September 2021)

Recent experiments on quantum walks (QWs) demonstrated a full control over the statistics-dependent walks of single particles and two particles in one-dimensional lattices. However, little is known about the general characterization of QWs at the many-body level. Here, we rigorously study QWs, Bloch oscillations, and the quantum Fisher information for three indistinguishable bosons and fermions in one-dimensional lattices using a time-evolving block decimation algorithm and many-body perturbation theory. We show that such strongly correlated QWs not only give rise to statistics-and-interaction-dependent ballistic transports of scattering states and of two- and three-body bound states but also allow a quantum enhanced precision measurement of the gravitational force. In contrast to the QWs of the fermions, the QWs of three bosons exhibit strongly correlated Bloch oscillations, which present a surprising time scaling t^3 of the Fisher information below a characteristic time t_0 and saturate to the fundamental limit of t^2 for $t > t_0$.

DOI: 10.1103/PhysRevLett.127.100406

Quantum walks (QWs) [1,2], the quantum counterpart of the classical random walks, are characterized by a fast ballistic spreading with wave fronts expanding linearly in time. Owing to their nonclassical features, they have potential applications in quantum algorithms [3], quantum computing [4], quantum information [5,6], quantum simulation [7], and quantum biology [8]. QWs have been experimentally implemented in a variety of quantum systems [9] and recently found in detecting topological states [10–12], discrete-time QWs [13–16], and bound states of magnons [17,18].

Up to now, most previous works focused on the one- and two-particle QWs in one-dimensional (1D) lattices. Preliminary experiments studied the QWs of a single particle and two particles by using either neutral atoms [19], ions [20], photons [21], spin impurities [18,22], or nuclear-magnetic-resonance systems [23]. Walkers of two noninteracting particles can develop nontrivial correlations due to the Hanbury-Brown-Twiss interference [24–30]. Bosonic (fermionic) walkers result in an emergence of bunching (antibunching) in density-density correlations [31–34], and anyons are in between [35,36]. Moreover, the interplay between quantum statistics and the interaction of two particles [33,34,37–43], and of two and three flipped spins in a Heisenberg chain [44], leads to a richer dynamics of quantum cowalking.

On the other hand, a quantum particle in a tilted periodic potential may undergo Bloch oscillation (BO), which has been demonstrated via ultracold atoms [34,45]. The BO frequency is proportional to the tilting force. This can be employed to measure the gravitational force [46,47], the magnetic field gradient [48], the Zak phase in topological Bloch bands [49], and the Casimir-Polder force [50]. Quantum Fisher information (FI), which provides a lower limit to the Cramér-Rao bound, plays a central role in quantum precision measurements [51–53]. However, the question of how to create many-body entanglement to improve measurement precision via BOs and how to use the FI to quantify the precision limit for the gravitational force still remains open and challenging.

In this Letter, we study the nonequilibrium dynamics of three fermions and three bosons in 1D lattices and explore its metrological application in the precision measurement of gravitational force. Continuous-time QWs, strongly

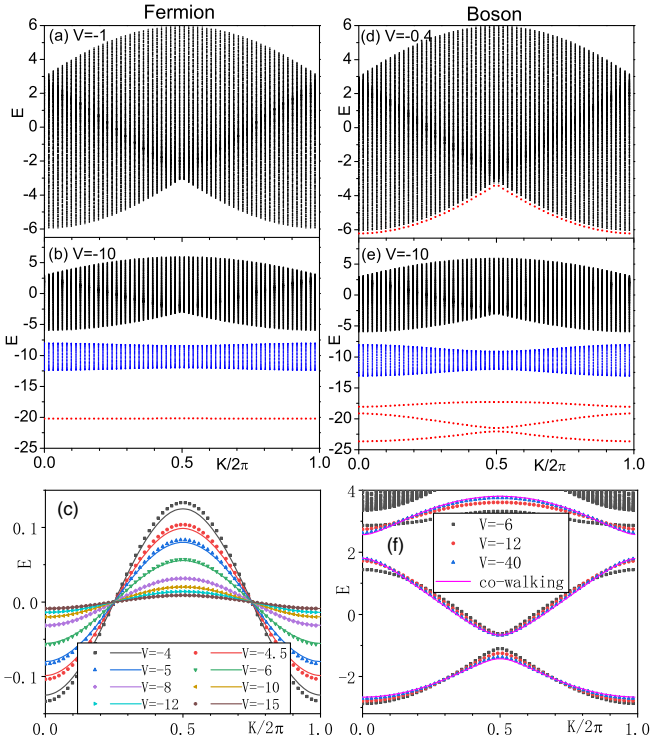

FIG. 1. The spectra of three fermions (a),(b) and three bosons (d),(e) for $L = 61$ and different values of interaction strength. Each point represents an eigenenergy E for a given total momentum K, and the red and blue dots correspond to the energies of three- and two-body bound states, respectively. (c) and (f) show the spectra of the 3BSs of fermions and bosons, respectively. The solid lines denote the perturbation results of Eqs. (2) and (3), which agree well with the ED calculation (symbols). All spectra in either (c) or (f) are shifted by a constant.

correlated BOs, the band structure, time evolutions of density distributions, and density-density correlations for the systems are thoroughly studied through numerical and analytical methods. The FI of such QWs shows a promising capability for quantum-enhanced precision measurement of weak forces in the walks of three-boson bound states.

The model.—We consider three indistinguishable particles moving on 1D lattices governed by the following Hamiltonian:

$$\hat{H} = -J \sum_{j=-M}^{M-1} (a_j^\dagger a_{j+1} + \text{H.c.}) + V \sum_{j=-M}^{M-1} \hat{n}_j \hat{n}_{j+1}. \quad (1)$$

Here, $a_j^\dagger$ (a_j) creates (annihilates) a particle at the jth site, and $\hat{n}_j = a_j^\dagger a_j$ is the particle number operator. The total number of lattice sites $L = 2M$. J is the nearest-neighbor hopping and sets the unit of energy ($J = 1$). V is the nearest-neighbor interaction. Hamiltonians like Eq. (1) can be realized with ultracold atoms [34,54,55]. Here, we study two types of particles: bosons and fermions. The fermionic model is equivalent to the exactly solvable XXZ Heisenberg chain [56–58], which is also equivalent to the hard-core bosonic model [59]. The QW of two and three particles of the XXZ model was found in [44], and an experimental realization via ultracold two-level atoms in deep optical lattices was given in [33,48,60].

Spectra and quantum walks.—Within the three-particle Hilbert space, we first perform exact diagonalization (ED) of the systems in momentum space. Figure 1 shows the spectra of three fermions and bosons, respectively. We observe that the three-particle systems of bosons and fermions host scattering states (SSs), two-body bound states (2BSs), and three-body bound states (3BSs). In the weak interaction region, the spectra only contain one continuum band corresponding to SSs for the three bosons and three fermions. However, as the attraction increases, the spectra behave in a rather statistics-dependent manner; see Figs. 1(a), 1(b), 1(d), 1(e). For the bosonic system, the bound states (BSs) split from the continuum band when the interaction V becomes stronger. The whole spectra contain three isolated spectra with gaps in between. Three minibands of the 3BSs, which are energetically lower than those of the 2BSs [blue part in Figs. 1(b), 1(e)], remarkably form competitive QWs in time evolution. The SS band is continuous with highest energies. In contrast, for the fermionic system, there is only one continuum SS band as long as the interaction $|V| < 1$. Bands of the SSs, 2BSs, and 3BSs are energetically separated for large attractions. The 3BSs only constitute one miniband with the lowest energy, which becomes more and more flat when the attraction increases.

Now we employ a time-evolving block decimation algorithm [40,61] to numerically simulate the three-particle continuous-time QWs. The QWs are governed by the unitary time evolution $|\psi(t)\rangle = e^{-iHt}|\psi(t=0)\rangle$, in contrast to the discrete-time QWs, which obey a successive single-time evolution governed by "shift" and "coin" operators [13–16]. Here, we set the initial state $|\psi(t=0)\rangle = a_{-1}^\dagger a_0^\dagger a_1^\dagger |0\rangle$ with three particles at the three central neighboring sites. Open boundary conditions are used under the cumulative truncation errors in the order of 10^{-8}. We study the time evolutions of density distribution $n_j(t) = \langle\psi(t)|a_j^\dagger a_j|\psi(t)\rangle$ and density-density correlation function $C_{i,j}(t) = \langle\psi(t)|\hat{n}_i\hat{n}_j|\psi(t)\rangle$, which preserve the symmetries $n_j(t)|_V = n_j(t)|_{-V}$ and $C_{i,j}(t)|_V = C_{i,j}(t)|_{-V}$ [62,63]. We thus only consider the attractive interaction in our study.

In Fig. 2, we show the time evolutions of density distribution for three-particle QWs. Both the weakly interacting bosons and fermionic systems with $|V| < 1$ have the same form of evolution, i.e., a single ballistic expansion light cone is established because of the single continuum band of the SSs. For the fermionic system with the interaction $|V| > 1$, an inner cone emerges with a slower and linearly moving wave front, indicating the

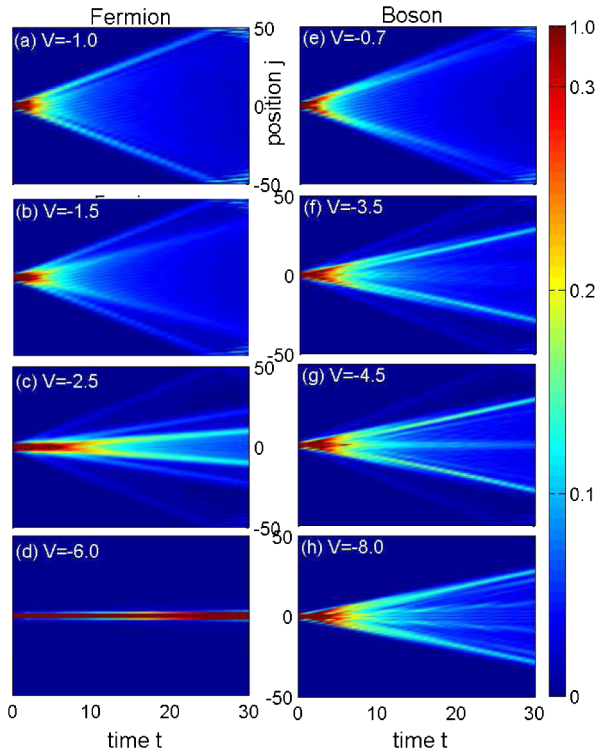

FIG. 2. Time evolutions of density distribution for three fermion (a)–(d) and three boson (e)–(h) systems with $L = 101$ and different values of attractions; see text. Results (a)–(d) match the analytic results for the XXZ Heisenberg model [44].

formation of BSs. Continuing to increase the interaction, the third innermost cone forms. From outer to inner, three cones correspond to ballistic expansions of the SSs, 2BSs, and 3BSs, respectively; see Fig. 2(c). As $|V|$ is further increased, the cones of the SSs and 2BSs gradually fade away and only the light cone of the 3BSs remains. The speed of wave front (SWF) of the SSs is independent of interaction, i.e., it is always 2, showing a maximal group velocity (MGV) of noninteracting particles. However, the SWFs for 2BSs and 3BSs decrease when the interaction $|V|$ increases. Note that the results of Figs. 2(a)–2(d) for fermions nicely match the corresponding analytic results for the equivalent XXZ Heisenberg model [44].

For the bosonic system, besides the outer cone for the SSs, an inner cone for the BSs emerges as long as V is nonzero. When the interaction increases, the SWF of this inner cone first decreases and then stops decreasing at a fixed value due to the band structure of the 3BSs. Then the third innermost cone shows up. Its SWF first decreases and then increases to a finite value; see Figs. 2(f)–2(h) and Fig. S9 in [63]. This unique behavior of the innermost cone is caused by the interplay of the 2BS and the 3BS. For a large enough attraction, the evolution contains only two cones, which are both related to the three minibands of the 3BSs.

Moreover, the density-density correlation function $C_{i,j}(t)$ also provides an important statistical nature of the

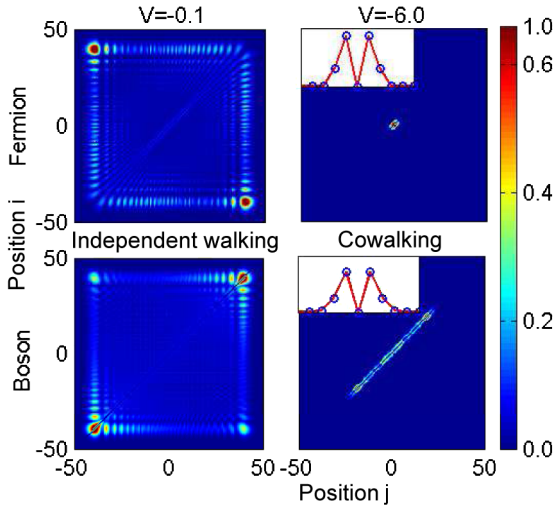

FIG. 3. Density-density correlation functions $C_{i,j}$ for both the fermionic (upper panel) and bosonic (lower panel) systems with a size $L = 101$ at the time $t = 22$. Corresponding profiles $C_{i=0,j}$ around $j = 0$ are shown in subsets.

three-particle QWs [63]. It significantly marks the difference between cowalking and individual walking. The cowalking particles bind together and move as a single composite particle, revealing the togetherness of quasiparticles. The density-density correlations for cowalking show few lines (5 lines) at $(i = j \pm d)$ with $d = 1, 2$ in the (i, j) plane, a signature of the cowalking. In Fig. 3, we show $C_{i,j}(t)$ for both the fermionic and bosonic systems at time $t = 22$ (they are free from the boundary effects). For a small $|V|$, the correlation function shows (anti-)bunching behavior with (off-)diagonal correlations at the wave front in the (fermionic) bosonic system. As $|V|$ increases, bunching and antibunching correlations fade away, and correlations on four minor diagonal lines $(i = j \pm 1,\ 2)$ are gradually enhanced with respect to a statistics-dependent pace; see the subsets in Fig. 3. In contrast to the cowalking of two bosons [33], the cowalking of three bosons remarkably shows expansive wave fronts due to the existence of the minibands of the 3BSs.

Many-body perturbation and Bloch oscillations.—Under a strong attraction, one can treat the hopping as a perturbation to the interaction term in the Eq. (1) Hamiltonian; see [57]. After projecting onto the subspace of the 3BSs, an effective single-particle model can be derived explicitly. For the fermionic case, by using the third order perturbation, an effective single-particle Hamiltonian for the cowalking of three fermions is given by [63]

$$\hat{H}^{\mathrm{F}}_{\mathrm{eff}} = -\frac{J^3}{V^2}\sum_j (c_j^\dagger c_{j+1} + \mathrm{H.c.}), \tag{2}$$

where $c_j^\dagger = a_{j-1}^\dagger a_j^\dagger a_{j+1}^\dagger$. The spectrum of this single-particle Hamiltonian reads $E^{\mathrm{F}}_{\mathrm{eff}}(K) = -(2J^3/V^2)\cos(K)$

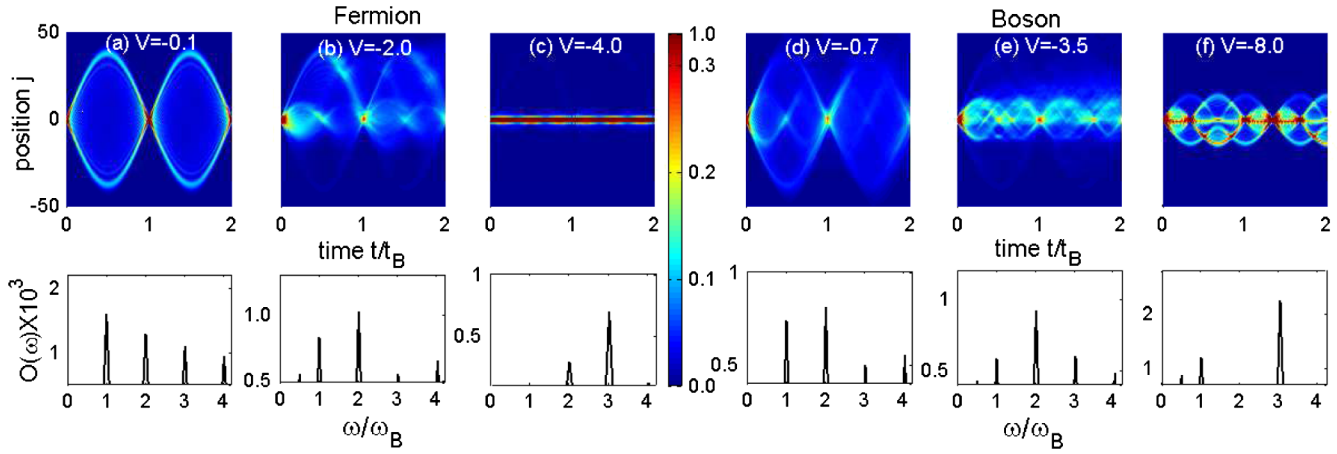

FIG. 4. Left (a)–(c) and right (d)–(f) panels show the time evolutions of density distributions for three bosons and three fermions with $L = 101$ and $F = 0.1$, respectively. Multiple fractional Bloch oscillations are observed. The corresponding frequencies are shown in the bottom row.

with a MGV $v^{\mathrm{F}} = 2J^3/V^2$; see [64]. In Fig. 1(c), we show the spectrum of the 3BSs for the fermionic system, where the dots denote the numerical result obtained from ED, and the lines are obtained from the effective single-particle Hamiltonian [Eq. (2)]. Both results agree well as $|V|$ increases. The MGV v^F is also in a good agreement with the SWF of the 3BSs [63]. We observe from Eq. (2) that the ballistic expansion of three-fermion cowalking becomes very slow as $|V|$ increases.

The subspace of three-boson cowalking has $3L$-fold degeneracies. The first order perturbation gives an effective single-particle Hamiltonian [63]:

$$\hat{H}^B_{\mathrm{eff}} = -\sqrt{2}J\sum_j (d_j^\dagger b_j + c_j^\dagger b_j + \sqrt{2}d_{j+1}^\dagger c_j + \mathrm{H.c.}) \qquad (3)$$

with three species: $b_j^\dagger = a_{j-1}^\dagger a_j^\dagger a_{j+1}^\dagger$, $c_j^\dagger = (1/\sqrt{2})(a_j^\dagger)^2 a_{j+1}^\dagger$, and $d_j^\dagger = (1/\sqrt{2})a_{j-1}^\dagger (a_j^\dagger)^2$. Obviously, the single-particle Hamiltonian (3) is independent of V. In the momentum space, we can get the spectra of the effective Hamiltonian [Eq. (3)], which are shown in Fig. 1(f) (solid lines) and agree well with the ED numerical results (dotted lines). The 3BSs have three minibands that show two different MGVs: $v_1^B \simeq 1$ for the middle miniband and $v_2^B \simeq 0.64$ for the other two minibands in Fig. 1(f) (solid lines). $v_{1(2)}^B$ agrees well with the SWF of the outer (inner) cone when $|V| \gg 1$; see [63].

In order to achieve a metrological application of QWs, we add a static force to the Eq. (1) Hamiltonian:

$$\hat{H}_{\mathrm{Force}} = F\sum_j j a_j^\dagger a_j \qquad (4)$$

with F the strength of the applied force and consider the BOs from the same initial state $|\psi(t=0)\rangle = a_{-1}^\dagger a_0^\dagger a_1^\dagger |0\rangle$.

We illustrate the BOs for fermionic systems in the left panel of Fig. 4. For a weak interaction, i.e., $|V| < 1$, particles independently undergo a single-particle BO with the amplitude $4J/F$ and the temporal period $t_B = 2\pi/F$ (frequency $\omega_B = F$) [65,66]. When $|V| > 1$, two inner BOs appear successively with smaller amplitudes and shorter periods. From outer to inner, there are BOs for the SSs, 2BSs, and 3BSs, respectively. Upon further increasing the attraction, the two outer BOs gradually fade away and only the BO of the 3BSs remains; see [63]. In order to analyze the periodicity, we introduce a density difference $O(t) = \sum_j |n_j(t) - n_j(t=0)|/L$. From the Fourier transformation $O(\omega)$, we observe the characteristics periodicities of $t_B/2$ and $t_B/3$ (or frequencies $2\omega_B$ and $3\omega_B$) BOs for the 2BSs and 3BSs, respectively, which are called fractional BOs in interacting systems [67–69]. $O(\omega)$ presents the relative weights of BO modes with different frequencies. In the strong coupling limit, i.e., $|V| \gg 1$, the co-BO of the 3BSs of fermions can be described by the effective single-particle Hamiltonian $\hat{H}^F_{\mathrm{BO}} = \hat{H}^F_{\mathrm{eff}} + 3F\sum_j j c_j^\dagger c_j$ with the BO amplitude $4J^3/(3V^2F)$, which is inversely proportional to V^2. Here, the effective force is $3F$, which leads to the periodicity of co-BO $t_B/3$, as well as the frequency of $3\omega_B$.

Because of the quantum statistical difference, the ground-state degeneracies are different for bosons and fermions, leading to different many-body perturbation processes as well as different dynamics of the BOs; see Fig. 4. The corresponding effective single-particle Hamiltonian describing the BOs among three minibands under an effective force $3F$ is given by

$$\hat{H}^B_{\mathrm{BO}} = \hat{H}^B_{\mathrm{eff}} + 3F\sum_j \left[j b_j^\dagger b_j + \left(j + \frac{1}{3}\right) c_j^\dagger c_j + \left(j - \frac{1}{3}\right) d_j^\dagger d_j \right]; \qquad (5)$$

see [63]. We observe that the Landau-Zener tunnelings display between two nearby minibands [70,71]. The amplitude of co-BO $\propto J/3F$ is independent of V, showing a larger FI than that of the cowalking of three fermions in the next section. Consequently, the periodicity of the co-BO of three bosons is $t_B/3$ and the frequency is $3\omega_B$, which provides an ideal metrological state for a precision measurement of a weak force.

Fisher information and precision measurement.—The three-boson QWs have a very rich dynamical structure of the co-BOs that leads to an almost interaction-independent co-BO amplitude and high value of FI in the probe of the weak force; see [63]. Here, the FI for (co-)BOs presents the precision limit for the single parameter F. By definition of FI for a unitary process from a pure initial state [53,72,73], we can calculate the FI of single-particle and multiparticle (co-)BOs [63]:

$$\begin{aligned}\mathcal{F} &= 4\left\{\left[\frac{\partial}{\partial F}\langle\psi(t)|\right]\frac{\partial}{\partial F}|\psi(t)\rangle - |\langle\psi(t)|\frac{\partial}{\partial F}|\psi(t)\rangle|^2\right\},\\ &= 4t^2\Delta H^{Q}(t),\end{aligned} \tag{6}$$

where $\Delta H^{Q}(t)$ is the fluctuation of a time-dependent effective Hamiltonian $H^{Q}(t)$ over the initial state $|\psi_0\rangle$:

$$\begin{aligned}\Delta H^{Q}(t) &= \langle\psi_0|[H^{Q}(t)]^2|\psi_0\rangle - \langle\psi_0|H^{Q}(t)|\psi_0\rangle^2,\\ H^{Q}(t) &= h[it\cdot \mathrm{ad}_{H_{\mathrm{BO}}}](\partial_F H_{\mathrm{BO}})\end{aligned} \tag{7}$$

with operator function $h[x] = (e^x - 1)/x$ and adjoint operator $\mathrm{ad}_G(C) = [G, C]$. In Fig. 5, we show the FI as functions of time for the (co)-BOs. Here we denoted single-particle (S), two-boson (2B), two-fermion (2F), three-fermion (3F), and three-boson (3B) (co-)BOs, respectively. We demonstrate that below a characteristic time $t_0 \approx 0.5t_B$, the time scalings of the FI show a surprising power-law form $\mathcal{F} \simeq \alpha t^3$, where α is a state-dependent constant [74]; also see [63]. In contrast to the smallest FI of the three-fermion co-BO with $\alpha \approx 0.024$, the three-boson co-BO has the FI with the largest value of $\alpha \approx 1185.485$ and then the smallest uncertainty in the measurement of force. The single-particle BO has the second largest FI. For $t > t_0$, the FI for these walk states saturates to the standard quantum limit $\mathcal{F} \simeq 4At^2$ with case-dependent constant coefficients A.

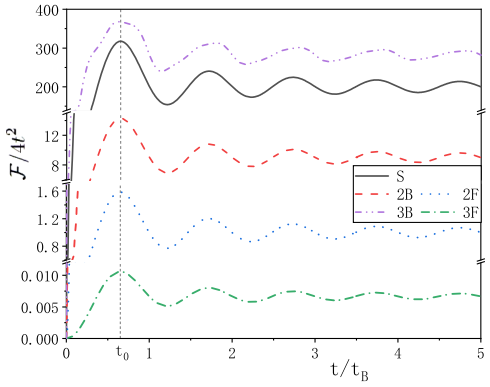

FIG. 5. The time-dependent quantum FI $\mathcal{F}/4t^2$ vs time t for single-particle and multiparticle (co)-BOs. Parameters: $L = 101$, $V = -10$, and $F = 0.1$. The FI is proportional to t^3 for $t < t_0$, while $\mathcal{F} \sim t^2$ for $t > t_0$.

Conclusions and discussions.—We have studied continuous-time QWs, BOs, and the FI of three bosons and three fermions in 1D lattices, which reveals the intrinsic and extrinsic roles of quantum statistics, interaction, and the gravitational force in the quantum random walks. We have demonstrated that the metrological useful entanglement for high precision measurements of weak forces can be generated under the time evolutions of suitable quantum states. Our method also holds promise for a quantum-enhanced precision test of the equivalence principle (EP) through the QWs of three bosons.

The superiority of three-boson co-BO in precision measurement of weak force would provide a potential approach to test the Einstein EP. Instead of making a comparison to the BOs of noninteracting isotopes [47], one may test the EP through the BOs of the same species of three interacting bosons; see the discussion in [63].

This work is supported by the National Key R&D Program of China No. 2017YFA0304500 and the NKRDP under Grant No. 2016YFA0301503, the NSFC Grants No. 11874393, No. 1167420, and No. 12025509. The authors thank Jing Liu and Wei-Dong Li for helpful discussions.

X. M. C., H. T. Y., and H. L. S. contributed equally to the numerical and analytical studies for this research.

*Corresponding author.
lichaoh2@mail.sysu.edu.cn
†Corresponding author.
xwe105@physics.anu.edu.au

[1] Y. Aharonov, L. Davidovich, and N. Zagury, Phys. Rev. A **48**, 1687 (1993).
[2] J. Kempe, Contemp. Phys. **44**, 307 (2003).
[3] A. Ambainis, Int. J. Quantum. Inform. **01**, 507 (2003).
[4] A. M. Childs, D. Gosset, and Z. Webb, Science **339**, 791 (2013).
[5] F. Zatelli, C. Benedetti, and M. G. A. Paris, Entropy **22**, 1321 (2020).
[6] S. E. Venegas-Andraca, Quantum Inf. Process. **11**, 1015 (2012).
[7] J. K. Asbóth, Phys. Rev. B **86**, 195414 (2012).
[8] S. Lloyd, J. Phys. Conf. Ser. **302**, 012037 (2011).
[9] J. Wang and K. Manouchehri, *Physical Implementation of Quantum Walks* (Springer, Berlin, Heidelberg, 2013).
[10] T. Kitagawa, M. A. Broome, A. Fedrizzi, M. S. Rudner, E. Berg, I. Kassal, A. Aspuru-Guzik, E. Demler, and A. G. White, Nat. Commun. **3**, 882 (2012).

[11] Y. E. Kraus, Y. Lahini, Z. Ringel, M. Verbin, and O. Zilberberg, Phys. Rev. Lett. **109**, 106402 (2012); M. Verbin, O. Zilberberg, Y. E. Kraus, Y. Lahini, and Y. Silberberg, Phys. Rev. Lett. **110**, 076403 (2013).

[12] V. V. Ramasesh, E. Flurin, M. Rudner, I. Siddiqi, and N. Y. Yao, Phys. Rev. Lett. **118**, 130501 (2017).

[13] C. Destri and H. J. De Vega, Nucl. Phys. **B290**, 363 (1987).

[14] C. Cedzich, T. Rybár, A. H. Werner, A. Alberti, M. Genske, and R. F. Werner, Phys. Rev. Lett. **111**, 160601 (2013).

[15] A. Bisio, G. M. D'Ariano, P. Perinotti, and A. Tosini, Phys. Rev. A **97**, 032132 (2018).

[16] P. Arnault, B. Pepper, and A. Pérez, Phys. Rev. A **101**, 062324 (2020).

[17] A. Ahlbrecht, A. Alberti, D. Meschede, V. B. Scholz, A. H. Werner, and R. F. Werner, New J. Phys. **14**, 073050 (2012).

[18] T. Fukuhara, P. Schauß, M. Endres, S. Hild, M. Cheneau, I. Bloch, and C. Gross, Nature (London) **502**, 76 (2013).

[19] M. Karski, L. Förster, J.-M. Choi, A. Steffen, W. Alt, D. Meschede, and A. Widera, Science **325**, 174 (2009).

[20] H. Schmitz, R. Matjeschk, C. Schneider, J. Glueckert, M. Enderlein, T. Huber, and T. Schaetz, Phys. Rev. Lett. **103**, 090504 (2009); F. Zähringer, G. Kirchmair, R. Gerritsma, E. Solano, R. Blatt, and C. F. Roos, Phys. Rev. Lett. **104**, 100503 (2010).

[21] A. Schreiber, K. N. Cassemiro, V. Potoček, A. Gábris, P. J. Mosley, E. Andersson, I. Jex, and C. Silberhorn, Phys. Rev. Lett. **104**, 050502 (2010); M. A. Broome, A. Fedrizzi, B. P. Lanyon, I. Kassal, A. Aspuru-Guzik, and A. G. White, Phys. Rev. Lett. **104**, 153602 (2010); A. Schreiber, K. N. Cassemiro, V. Potoček, A. Gábris, I. Jex, and C. Silberhorn, Phys. Rev. Lett. **106**, 180403 (2011).

[22] T. Fukuhara, A. Kantian, M. Endres, M. Cheneau, P. Schauß, S. Hild, D. Bellem, U. Schollwöck, T. Giamarchi, C. Gross, I. Bloch, and S. Kuhr, Nat. Phys. **9**, 235 (2013).

[23] J. Du, H. Li, X. Xu, M. Shi, J. Wu, X. Zhou, and R. Han, Phys. Rev. A **67**, 042316 (2003).

[24] A. Peruzzo, M. Lobino, J. C. F. Matthews, N. Matsuda, A. Politi, K. Poulios, X. Zhou, Y. Lahini, Nur Ismail, K. Wörhoff, Y. Bromberg, Y. Silberberg, M. G. Thompson, and J. L. OBrien, Science **329**, 1500 (2010).

[25] K. Mayer, M. C. Tichy, F. Mintert, T. Konrad, and A. Buchleitner, Phys. Rev. A **83**, 062307 (2011).

[26] R. H. Brown and R. Q. Twiss, Nature (London) **177**, 27 (1956).

[27] M. Hillery, Science **329**, 1477 (2010).

[28] L. Sansoni, F. Sciarrino, G. Vallone, P. Mataloni, A. Crespi, R. Ramponi, and R. Osellame, Phys. Rev. Lett. **108**, 010502 (2012).

[29] A. S. Solntsev, A. A. Sukhorukov, D. N. Neshev, and Y. S. Kivshar, Phys. Rev. Lett. **108**, 023601 (2012).

[30] Y. Lahini, M. Verbin, S. D. Huber, Y. Bromberg, R. Pugatch, and Y. Silberberg, Phys. Rev. A **86**, 011603(R) (2012).

[31] Y. Omar, N. Paunkovič, L. Sheridan, and S. Bose, Phys. Rev. A **74**, 042304 (2006).

[32] C. Benedetti, F. Buscemi, and P. Bordone, Phys. Rev. A **85**, 042314 (2012).

[33] X. Qin, Y. Ke, X. Guan, Z. Li, N. Andrei, and C. Lee, Phys. Rev. A **90**, 062301 (2014).

[34] P. M. Preiss, R. Ma, M. E. Tai, A. Lukin, M. Rispoli, P. Zupancic, Y. Lahini, R. Islam, and M. Greiner, Science **347**, 1229 (2015).

[35] L. Wang, L. Wang, and Y. Zhang, Phys. Rev. A **90**, 063618 (2014).

[36] L. L. H. Lau and S. Dutta, arXiv:2012.03977.

[37] M. Ganahl, E. Rabel, F. H. L. Essler, and H. G. Evertz, Phys. Rev. Lett. **108**, 077206 (2012).

[38] P. L. Krapivsky, J. M. Luck, and K. Mallick, J. Phys. A **48**, 475301 (2015).

[39] D. Wiater, T. Sowiński, and J. Zakrzewski, Phys. Rev. A **96**, 043629 (2017).

[40] D. Iyer, H. Guan, and N. Andrei, Phys. Rev. A **87**, 053628 (2013).

[41] I. Siloi, C. Benedetti, E. Piccinini, J. Piilo, S. Maniscalco, M. G. A. Paris, and P. Bordone, Phys. Rev. A **95**, 022106 (2017).

[42] A. Beggi, I. Siloi, C. Benedetti, E. Piccinini, L. Razzoli, P. Bordone, and M. G. A. Paris, Eur. J. Phys. **39**, 065401 (2018).

[43] S. Sarkar and T. Sowiński, Phys. Rev. A **102**, 043326 (2020).

[44] W. Liu and N. Andrei, Phys. Rev. Lett. **112**, 257204 (2014).

[45] Z. A. Geiger, K. M. Fujiwara, K. Singh, R. Senaratne, S. V. Rajagopal, M. Lipatov, T. Shimasaki, R. Driben, V. V. Konotop, T. Meier, and D. M. Weld, Phys. Rev. Lett. **120**, 213201 (2018).

[46] G. Ferrari, N. Poli, F. Sorrentino, and G. M. Tino, Phys. Rev. Lett. **97**, 060402 (2006).

[47] M. G. Tarallo, T. Mazzoni, N. Poli, D. V. Sutyrin, X. Zhang, and G. M. Tino, Phys. Rev. Lett. **113**, 023005 (2014).

[48] W. Liu, Y. Ke, L. Zhang, and C. Lee, Phys. Rev. A **99**, 063614 (2019).

[49] M. Atala, M. Aidelsburger, J. T. Barreiro, D. Abanin, T. Kitagawa, E. Demler, and I. Bloch, Nat. Phys. **9**, 795 (2013).

[50] I. Carusotto, L. Pitaevskii, S. Stringari, G. Modugno, and M. Inguscio, Phys. Rev. Lett. **95**, 093202 (2005).

[51] C. W. Helstrom, *Quantum Detection and Estimation Theory* (Academic Press, New York, 1976).

[52] L. Pezzè, A. Smerzi, M. K. Oberthaler, R. Schmied, and P. Treutlein, Rev. Mod. Phys. **90**, 035005 (2018).

[53] J. Liu, H. Yuan, X. M. Lu, and X. Wang, J. Phys. A **53**, 023001 (2020).

[54] H. Sun, B. Yang, H. Y. Wang, Z. Y. Zhou, G. X. Su, H. N. Dai, Z. S. Yuan, and J. W. Pan, Nat. Phys. (2021), https://doi.org/10.1038/s41567-021-01277-1.

[55] B. Yang, H. Sun, R. Ott, H. Y. Wang, T. V. Zache, J. C. Halimeh, Z. S. Yuan, P. Hauke, and J. W. Pan, Nature (London) **587**, 392 (2020).

[56] C. N. Yang and C. P. Yang, Phys. Rev. **150**, 321 (1966); **150**, 327 (1966); **151**, 258 (1966).

[57] M. Takahashi, J. Phys. C **10**, 1289 (1977).

[58] M. Takahashi, *Thermodynamics of One-Dimensional Solvable Models* (Cambridge University Press, Cambridge, 1999).

[59] P. Jordan and E.Wigner, Z. Phys. **47**, 631 (1928).

[60] C. Lee, Phys. Rev. Lett. **93**, 120406 (2004).

[61] G. Vidal, Phys. Rev. Lett. **91**, 147902 (2003); **93**, 040502 (2004).
[62] J. Yu, N. Sun, and H. Zhai, Phys. Rev. Lett. **119**, 225302 (2017).
[63] See Supplemental Material at http://link.aps.org/supplemental/10.1103/PhysRevLett.127.100406 for more details on the symmetries in dynamic evolution, the correlation functions in three-particle QWs, the derivation of effective single-particle models for cowalkings and co-BOs, the two-body physics in three-particle QWs, the calculation of Fisher information, and additional figures for spectra, QWs, and BOs.
[64] The third-order amplitude is proportional to J^3/V^2. The fourth and higher orders are also nontrivial, but their amplitudes are much smaller than the third order when $J/V \ll 1$.
[65] Y. A. Kosevich and V. V. Gann, J. Phys. Condens. Matter **25**, 246002 (2013).
[66] H. Zhang, Y. Zhai, and X. Chen, J. Phys. B **47**, 025301 (2014).
[67] W. S. Dias, E. M. Nascimento, M. L. Lyra, and F. A. B. F. de Moura, Phys. Rev. B **76**, 155124 (2007).
[68] R. Khomeriki, D. O. Krimer, M. Haque, and S. Flach, Phys. Rev. A **81**, 065601 (2010).
[69] G. Corrielli, A. Crespi, G. Della Valle, S. Longhi, and R. Osellame, Nat. Commun. **4**, 1555 (2013).
[70] B. M. Breid, D. Witthaut, and H. J. Korsch, New J. Phys. **8**, 110 (2006).
[71] S. Longhi, Phys. Rev. B **86**, 075144 (2012).
[72] S. L. Braunstein and C. M. Caves, Phys. Rev. Lett. **72**, 3439 (1994).
[73] S. L. Braunstein, C. M. Caves, and G. J. Milburn, Ann. Phys. (N.Y.) **247**, 135 (1996).
[74] The numerical values $\alpha = 1185.485$, 720.741, 32.434, 3.604, 0.024 for the states 3B, S, 2B, 2F, 3F, respectively. The errors of such power-law simulations are less than 3%.